

Optimization of a piezoelectric bimorph grasper for use in minimally invasive surgical applications

M Grujicic*, C L Zhao, and E M Austin

Department of Mechanical Engineering, Clemson University, Clemson, South Carolina, USA

The manuscript was received on 7 June 2004 and was accepted after revision for publication on 10 June 2005.

DOI: 10.1243/095440505X32607

Abstract: The potential use of piezoelectric bimorph actuators in minimally invasive surgery suture-needle grasper/holder applications is explored computationally. Upon defining the design/functional requirements for such surgical tools, a finite element analysis of the underlying piezoelectric boundary value problem is combined with the genetic algorithm optimization routine to arrive at an optimal morphology of the suture-needle grasper/holder. The results obtained show that, if the actuator is based on several constant-thickness segments, a proper combination of thicknesses of such segments can substantially improve the performance of such surgical tools. Specifically, a good combination of the relatively large grasper-jaws opening and the required level of the holding force when the grasper is closed on a 0.5 mm diameter suture-needle is obtained. The effect of orientation of the poling direction in the piezoelectric layers on the performance of the bimorph actuator is also examined. It is found that, at the same level of the required grasping force, a change in the poling direction by about 2.37° from the through-the-thickness direction can increase the maximum grasper-jaws opening by about 10 per cent.

Keywords: piezoelectric bimorph actuators, minimally invasive surgery, genetic algorithm

1 INTRODUCTION

The word 'piezoelectric' is made up of two parts: 'piezo', which is derived from the Greek word for pressure, and 'electric' from electricity. Thus, the piezoelectric effect pertains to the coupling between pressure and electric charge/field. Consequently, in a piezoelectric material, the application of a force or stress results in the development of an electrical charge/field in the material. This phenomenon is generally referred to as 'the direct piezoelectric effect'. Conversely, the application of an electric charge/field to the same material will result in a change of the physical dimensions, i.e. mechanical strain. This phenomenon is generally known as 'the converse piezoelectric effect'. Several ceramic materials such as lead-zirconate-titanate (PZT), lead-titanate (PbTiO_2), lead-zirconate (PbZrO_3), and barium-titanate (BaTiO_3) have been known to exhibit a piezoelectric effect. In addition, the piezoelectric

effect is found in a few polymers such as polyvinylidene fluoride (PVDF).

Piezoelectric materials contain micron-sized regions, generally referred to as the Weiss domains, which possess a permanent dipole moment. The orientation of such dipole moments in different Weiss domains in a virgin (un-poled) piezoelectric material is random and, hence, there is no net dipole moment at the macroscopic length scale. However, the application of a high electric field or a high stress (the process known as 'poling') causes the dipoles of different Weiss domains to align themselves with the principal direction of the applied field or stress, which gives rise to the polarization of the piezoelectric material. When the applied field/stress is removed, the domains tend to regain their initial polarization state, but this reversal is generally not complete and, as a result, a remnant polarization is generally found in the poled piezoelectric materials. Once piezoelectric materials are poled, the application of an electric field (generally substantially smaller in magnitude than the one used for poling of the material) can produce mechanical strains. This phenomenon enables piezoelectric materials to be

*Corresponding author: Department of Mechanical Engineering, Clemson University, 241 Fluor Daniel Building, Clemson, SC 29634-0921, USA. email: mica.grujicic@ces.clemson.edu

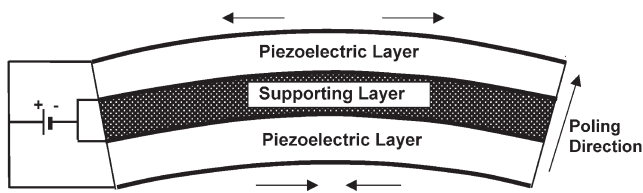


Fig. 1 A schematic of a piezoelectric bimorph actuator. Heavy lines on top and bottom of each layer are used to denote conductive metallic electrodes

used in electromechanical actuation applications. Furthermore, since the application of a mechanical force/stress gives rise to a build-up of the electric charge/field, these materials have also been used in mechanical sensing applications.

One of the most common ways in which piezoelectric materials are utilized in mechanical actuation applications is through the use of so-called 'piezoelectric bimorph actuators'. A schematic of a piezoelectric bimorph actuator is shown in Fig. 1. It can be described as a sandwich-type actuator in which two layers of a piezoelectric material are laminated onto one surface of a supporting beam or plate. The two piezoelectric layers are generally poled in the same direction, typically in the direction normal to the supporting beam/plate. When opposing electric fields are applied to the two piezoelectric layers, their corresponding dimensional changes are of the opposite character, which gives rise to bending of the beam/plate, Fig. 1. When two bimorph actuators are combined and driven by opposite electric fields, they can be used to create a simple grasping/holding device. A schematic of such a grasping device in its open and its fully-closed positions is shown in Figs 2(a)

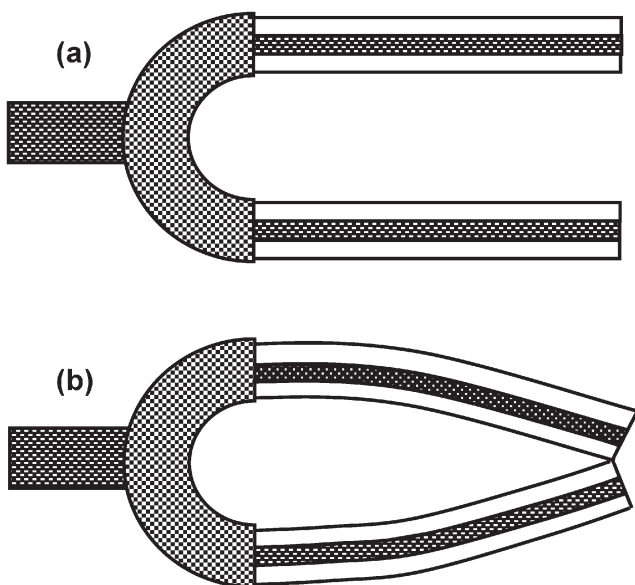


Fig. 2 A schematic of a piezoelectric bimorph grasper in the (a) open and (b) fully-closed positions

and (b), respectively. A number of researchers have investigated the potential of such grasping devices. Some of these investigations focus on the PZT-based bimorph actuators for the use in micro-electromechanical systems (MEMS) and in micro robots [e.g. 1–3], while the others have studied bimorph-actuator grippers based on piezoelectric polymers [e.g. 4, 5]. In addition, in a series of papers, Frecker and co-workers [6–8], explored the possibility of utilizing such grasping devices as surgical tools in minimally invasive surgeries.

Minimally invasive surgeries such as laparoscopy and endoscopy employ various miniature tools such as forceps, graspers, scissors, staples, needle holders, etc. Generally, such tools are designed as small, rigid end-effectors that are connected by mechanical hinge-joints and linked to a mechanical actuator via long tendon wires or push rods. Recently, a new generation of tools for the minimally invasive surgeries has been developed in which the concept of compliant structures/mechanisms-actuated electromechanically by smart-material actuators is utilized [e.g. 9, 10]. These tools are generally single-piece, flexible and rely on elastic deformation for transfer of the mechanical force and motion. The most important advantages of these tools over their rigid-link counterparts are: (a) an ease of manufacturing owing to their single-piece nature; (b) the elimination of the need of complicated millimeter length-scale assembly; (c) the elimination of cleaning of the hard-to-reach hinge areas; (d) an ease of integration with smart (actuating and sensing) materials such as high power-density and fast-response-time-piezoelectric ceramics.

The potential of flexible piezoelectric bimorphs in applications such as the suture-needle holder for minimally invasive surgery has been investigated numerically by Frecker and co-workers [6–8] using a metamodel-based optimization approach. While the work of Frecker and co-workers [6–8] is generally concerned with the key design/performance issues such as maximization of the jaws opening and the grasping force, their work primarily focuses on the design/optimization methodology aspects including: (a) a use of the design of experiments and metamodeling techniques to construct computationally inexpensive response surface approximations for the finite element simulations of piezoelectric bimorph actuators and (b) a use of the metamodels to generate rapidly the design space and identify the Pareto frontier for the competing design objectives of maximum deflection and maximum force. However, the issues associated with optimization of the design of a suture-needle holder/grasper are not completely addressed. In particular, the issues associated with finding a global optimum for the design space of a suture-needle holder/grasper.

The objective of the present work is to extend the investigation of Frecker and co-workers [6–8] related to the design optimization of a piezoelectric-bimorph-actuator-based suture-needle holder/grasper by utilizing a global optimization method, the genetic algorithm, in order to identify an optimum design of such a minimally invasive surgical tool.

The organization of the paper is as follows. A brief overview of the piezoelectric materials constitutive equations and the governing partial differential equations is presented in section 2.1. Functional requirements for the suture-needle holder and the definition of the corresponding boundary value problem are given in section 2.2. The computational method used to solve the boundary value problem is briefly discussed in section 2.3. The genetic algorithm method used for optimization of the needle-holder morphology is briefly reviewed in section 2.4. The results obtained in the present work are presented and discussed in section 3. The main conclusions resulting from the present work are summarized in section 4.

2 COMPUTATIONAL PROCEDURE

2.1 Piezoelectric materials constitutive equations and governing equations

The piezoelectric phenomenon described in the previous section is generally modelled as a linear interaction between the electrical and the mechanical processes. While a mathematical treatment of the piezoelectric phenomenon and its linear-theory analysis can be found in many standard sources (e.g. [11]), a brief overview of such treatment is given in this section to help the reader understand the finite element implementation presented in section 2.3. Using a condensed matrix notation, the stress versus the electrical field form of the piezoelectric constitutive equation can be written as

$$T = c^E S - e^t E \quad (1)$$

and

$$D = eS + \varepsilon^S E \quad (2)$$

where $T \in \mathbb{R}^{6 \times 1}$ is the mechanical stress vector, $S \in \mathbb{R}^{6 \times 1}$ the mechanical strain vector, $D \in \mathbb{R}^{3 \times 1}$ the electric displacement vector, $E \in \mathbb{R}^{3 \times 1}$ the electrical field vector, $c^E \in \mathbb{R}^{6 \times 6}$ the elastic stiffness matrix under constant electric field, the stress/field piezoelectric constant matrix, and $\varepsilon^S \in \mathbb{R}^{3 \times 3}$ the constant-strain permittivity matrix; a superscript t is used to denote the transpose of a matrix and $\mathbb{R}^{m \times n}$ denotes a real matrix of the size $m \times n$. Clearly, equations (1)–(2) can be reduced to the constitutive

equation for a linear elastic material under the conditions when both e and ε^S are zero matrices.

A summary of the piezoelectric and elastic properties of PZT, which is considered in the present work, is given in Appendix 2. It should be noted that the properties given in Appendix 2 are listed in accordance with the standard convention within which the poling direction is aligned with the 3-direction of the local material coordinate system. It should also be noted that the components of the T and S vectors are listed in the following order: (11, 22, 33, 12, 23, 13).

Since the Navier's mechanical equilibrium partial differential equation and the Gauss' law equation for the electrical equilibrium have similar mathematical forms, it is generally convenient to combine equations (1) and (2) into the following matrix equation:

$$\begin{bmatrix} T \\ D \end{bmatrix} = \begin{bmatrix} c^E & -e^t \\ e & \varepsilon^S \end{bmatrix} \begin{bmatrix} S \\ E \end{bmatrix} \quad (3)$$

The corresponding strain–electric field constitutive matrix equation can be readily defined as:

$$\begin{bmatrix} S \\ D \end{bmatrix} = \begin{bmatrix} s^E & d^t \\ d & \varepsilon^T \end{bmatrix} \begin{bmatrix} T \\ E \end{bmatrix} \quad (4)$$

where s^E is the constant-field compliance matrix, d the strain/field piezoelectric matrix, and ε^T is the constant-stress permittivity matrix. These three matrices are defined via the following equations:

$$c^E = [s^E]^{-1} \quad (5)$$

$$e = d[s^E]^{-1} \quad (6)$$

$$\varepsilon^S = \varepsilon^T - d[s^E]^{-1} d^t \quad (7)$$

The partial differential equations governing the behaviour of piezoelectric bimorph actuators include a mechanical equilibrium equation whose weak variational formulation can be expressed as [11]:

$$\begin{aligned} & 0.5 \int_{\Omega} (-S'_{11} T_{11} - S'_{22} T_{22} - S'_{33} T_{33} - 2S'_{12} T_{12} \\ & - 2S'_{23} T_{23} - 2S'_{13} T_{13}) d\omega + \int_S u^t F_s ds \\ & + \int_L u^t F_L dl + u^t F_p = 0 \end{aligned} \quad (8)$$

while the electrostatic equilibrium is defined by Maxwell's electrostatic equation:

$$-\frac{\partial D_1}{\partial x_1} - \frac{\partial D_2}{\partial x_2} - \frac{\partial D_3}{\partial x_3} = 0 \quad (9)$$

where a superscript prime is used to denote a test strain/displacement field, F denotes a force, while Ω (or ω), S (or s), L (or l), and P denote volume,

surface, line, and point quantities, respectively. x_1 , x_2 , and x_3 are the global coordinates.

Equations (8) and (9) are solved in the present work using a conventional displacement-based finite element method.

2.2 Formulation of the problems

2.2.1 Functional and design requirements

The objective of the present work is design and optimization of a PZT-based miniature grasper for use as a suture-needle holder in minimally invasive surgical applications. Minimally invasive surgeries generally rely on the use of several 3–10 mm long incisions in place of a single large incisions encountered in open surgeries. Consequently, minimally invasive surgeries offer the benefits associated with reduced tissue trauma and shorter patient recovery time [12, 13]. During minimally invasive surgeries, miniature surgical tools and viewing devices are introduced into the body cavity through long tubes with 5–10 mm diameter. Based on these considerations and simple estimates, the following functional/design requirements can be defined for a suture-needle piezoelectric bimorph grasper/holder:

- a maximum magnitude of the jaws opening in the fully open position of the holder to enable an easy grasp of the needle;
- jaws should be parallel when closed on a 0.5 mm diameter suture needle to prevent the needle from rolling;
- thickness and width should be such that the maximum cross-sectional dimension of the grasper does not exceed 90 per cent of the diameter of the tube through which the surgical tool is inserted into the body cavity;
- the grasper should exert a force between 0.4–0.6 N when the jaws are closed on the 0.5 mm diameter suture needle; and
- a short (ca. <200 ms) open/close response time.

The last functional requirement is automatically satisfied when ceramic piezoelectric materials such

as PZT are used for construction of the bimorph actuators.

According to the list of functional requirements described above, both the deflection and the force at the grasper jaws are critical. Their magnitudes are affected by the physical dimensions (length, width, and thickness) of the piezoelectric bimorph actuator and its piezoelectric and supporting layers, properties of the constituent materials, and the magnitude of the applied electrical voltage/field. When the piezoelectric bimorph actuator is based on constant-thickness piezoelectric layers, and under the assumption that the role of the supporting layer can be ignored, the tip deflection, δ , and the tip blocked force, F , can be defined using the simple strength of material relations as [11]:

$$\delta = \frac{0.75l^2 V d_{31}}{t^2} \quad (10)$$

and

$$F = 3d_{31} V \frac{tw}{l} Y_{11} \quad (11)$$

where l , w , and t are respectively the length, width, and thickness of a piezoelectric layer, V the voltage difference applied across one piezoelectric layer, d_{31} the 31 component of the strain/field piezoelectric matrix d , and Y_{11} the 11 component of the plane-strain elasticity constant. It should be noted that equations (10) and (11) define respectively a maximum displacement (in the absence of any resistance to the motion of the tip) and a maximum blocked force (corresponding to a zero value of the tip displacement).

At this point, it is important that the terms ‘the blocked force’ and ‘free-tip displacement’ are clearly defined as they are used throughout the remainder of this manuscript. When the right tip of the piezoelectric bimorph in Fig. 3 is constrained from moving in any direction, while the electrical voltage is applied, the constrained right tip of the bimorph develops a force. The component of this force in the through-the-thickness direction of the piezoelectric bimorph is referred as ‘the blocked force’. When the

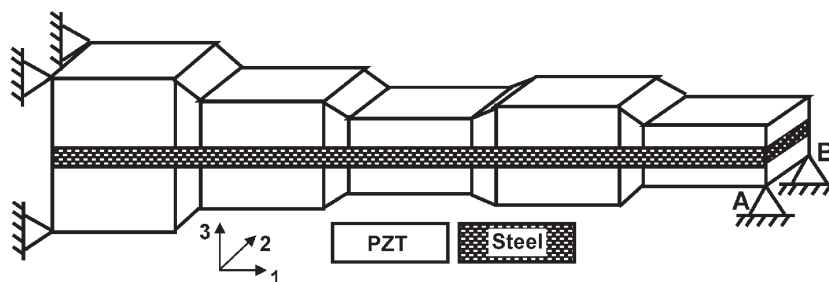


Fig. 3 A schematic of the three-dimensional formulation of the boundary value problem of a piezoelectric bimorph actuator. The constraints at points A and B are applied during the computation of the blocked force and are removed when the free-tip displacement is calculated

aforementioned constraints are removed from the right tip of the bimorph, this end is free to deflect as a result of the application of an electrical field. The component of this deflection in the through-the-thickness direction of the bimorph is referred to as 'free-tip displacement'.

2.2.2 Boundary value problem

Owing to the inherit symmetry of the piezoelectric-bimorph-actuator-based suture-needle grasper/holder, only one half of it is modelled in the present work. Consequently, the required blocked force needed to prevent needle roll is only one half (0.2–0.3 N) of the one given in the previous section. The one-half of the grasper (referred to as the piezoelectric bimorph actuator) is modelled as a composite beam with a constant-thickness steel supporting layer and non-uniform-thickness piezoelectric (top and bottom) layers. In the preliminary phase of this work, the thickness of the piezoelectric layers is considered to vary linearly with distance along the actuator length and the problem is reduced to a two-dimensional plane-strain formulation. In the main portion of the work presented here, however, each piezoelectric layer is considered to consist of five equal-length, fixed-thickness segments and the thicknesses of these layers are treated as design/optimization parameters. Constant-thickness piezoelectric layers are separated by linearly-varying-thickness thin piezoelectric layers. In addition, the problem is considered using a full three-dimensional formulation. A schematic of the three-dimensional formulation of the respective boundary value problem is given in Fig. 3.

The boundary conditions used in the present study are indicated in Fig. 3. It should be noted that the fixed boundary conditions applied to the right end of the piezoelectric bimorph as indicated in Fig. 3 are used only in the case when the blocked force is being calculated. These boundary conditions are removed when the free-tip displacement is calculated.

2.3 Computational method

The stationary system of governing partial differential equations (discussed in section 2.1) subjected to the boundary conditions (discussed in section 2.2) are implemented in the commercial mathematical package FEMLAB [14] and solved (for the dependent (displacements and charge densities) using the finite element method. The FEMLAB provides a powerful interactive environment for modelling various scientific and engineering problems and for obtaining the solution for the associated (stationary and transient, both linear and nonlinear) systems of governing partial differential equations. The FEMLAB is fully integrated with the MATLAB, a commercial

mathematical and visualization package [15]. As a result, the models developed in the FEMLAB can be saved as MATLAB programs for parametric studies or iterative design optimization. In the present work, an optimization algorithm known as the genetic algorithm is implemented in the MATLAB and interfaced with the finite element model developed using the FEMLAB program. A brief overview of the genetic algorithm is given in next section.

Standard mesh sensitivity and model robustness analyses are carried out following the procedure outlined in our recent work [16]. The results of these analyses validated that the model developed is mesh-insensitive and robust but, for the sake of brevity, the results are not presented here.

2.4 Genetic algorithm for parameter optimization

In this section of brief description is given of the procedure used to optimize the performance of piezoelectric bimorph actuators for use in the minimally invasive surgical suture-needle holder applications. The objective of the optimization process is to determine the thicknesses of the five piezoelectric segments which maximize the actuator-tip deflection while meeting all the functional/design requirements discussed in section 2.1. The question then becomes how to search efficiently the parameters' space for the combination of these five parameters which gives rise to a global maximum in the objective function (defined as the actuator-tip deflection), considering the fact that owing to a complex nature of the governing equations, the search space is probably multimodal (contains numerous local maximal of the objective function).

A review of the literature identifies three main types of search methods: (a) calculus-based; (b) enumerative, and (c) random methods. While generally very fast, calculus-based methods suffer from two main drawbacks: (i) they are local in scope, i.e. they typically locate the maximum which is highest (best) in the neighbourhood of the current search point; and (ii) they entail the knowledge of derivatives of the objective function whose evaluation (even through the use of numerical approximations) in multimodal and potentially discontinuous search spaces represents a series limitation. Within enumerative search methods, values of the objective function are evaluated at every preselected point in the research space, one a time. These methods generally require evaluation of the objective function at a large number of preselected points, which tends to make them inefficient and not very useful for problems of even moderate size and complexity.

Owing to the aforementioned shortcomings of the calculus-based and enumerative search methods, the genetic algorithm [17], one of the random

search methods, is used in the present work. Through (binary) coding, the genetic algorithm creates a parameter string (a chromosome set) for each considered point (individual) in the search space and utilizes the Darwinian principle of 'survival of the fittest' to ensure that chromosomes of the fittest individuals are retained (with a higher probability) in subsequent generations.

At the beginning of the genetic algorithm search procedure, a random selection of the parameters is used to create an initial population of individuals (parameter sets) of size n in the search space. The fitness (i.e. the objective function) is next computed for each of the individuals based on how well each individual performs (in its environment). To generate the next generation of individuals of the same population size, the genetic algorithm performs the following three operations: (1) selection, (2) crossover, and (3) mutation. Within the selection process, fitter individuals are selected (as parents) for mating, while weak individuals die off. Through mating, the parents create a child with a chromosome set that is some mix of the parents' chromosomes. Mixing of parents' chromosomes during child creation is referred to as 'crossover'. To promote evolution, a small probability is used to enable one or more child's chromosomes to mutate (change). The processes of child creation and mutation are continued until an entirely new population (of children) of size n is generated. The fitness of each child is determined and the processes of selection, crossover, and mutation repeated resulting in increasingly fitter generations of individuals. Additional details regarding parameter coding selection, crossover, and mutation as well as a logic flow chart for the genetic algorithm can be found in our previous work [18].

The genetic algorithm optimization method discussed above was implemented in MATLAB. Details of this implementation can be found in our previous work [18].

Within the present work, both the single-point crossover and the uniform crossover with a probability of 0.6 are considered. The results of the two types of simulations are found to be practically identical. Also, jump and creep mutations were used with the probabilities equal to an inverse of the population size. Furthermore, the elitism option was used to help prevent a random loss of good chromosome strings.

3 RESULTS AND DISCUSSION

3.1 Constant piezoelectric-layer thickness actuator

To demonstrate the trade-off between a piezoelectric-bimorph tip free displacement and the tip blocked

force, a series of plane-strain finite element analyses is carried out under the condition that the thickness of each piezoelectric layer does not vary along the actuator length. However, the piezoelectric-layer thickness is varied between 1 and 3 mm in increments of 0.25 mm between different runs. In all the calculations, the thickness of the supporting layer is kept fixed at 0.5 mm, while the length and the width of the piezoelectric layer is held constant at 10 mm and 3 mm, respectively. The length of each transition region is set to 1 mm, making the total length of the actuator equal to 54 mm. In all the simulations carried out in the present work, the supporting layer is considered to be made of steel which is modelled as an isotropic linearly elastic material with the Young's modulus, $E = 200$ GPa and the Poisson's ratio, $\nu = 0.3$. The width direction is chosen to correspond to the zero-strain direction. For each choice of the piezoelectric-layer thickness, two finite element analyses are carried out: (a) a free-tip deflection analysis within which no constraints are applied to the actuator right end and (b) a blocked-force analysis within which the actuator tip is fully constrained, and as voltage is applied, a force (the blocked force) is developed at the bimorph tip, since the tip is not allowed to deflect. The combined results of the two analyses displayed as a blocked force versus free-tip deflection plot are shown in Fig. 4. For comparison, the corresponding results obtained using the simple analytical model [equations (10) and (11)] and $d_{31} = 274 \times 10^{-12}$ m/V and $Y_{11} = 71$ GPa are also displayed in Fig. 4.

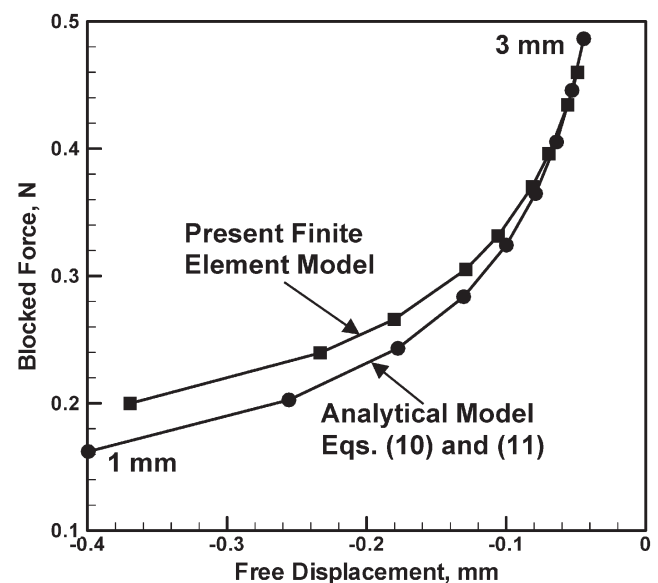


Fig. 4 A trade-off between the actuator-tip free displacement and the actuator-tip blocked force in bimorph actuators with a constant thickness of their piezoelectric layers. See text for details

The results displayed in Fig. 4 clearly show a trade-off between the tip free displacement and the tip blocked force. More specifically, a small thickness of the piezoelectric layers increases tip free displacement while the blocked force increases with an increase in the piezoelectric-layer thickness. These findings are consistent with the fact that a smaller thickness of the piezoelectric layer yields a higher electrical field and, hence, a lower displacement. At the same time, a thinner piezoelectric layer has a lower stiffness and hence, at the same level of actuator-tip displacement, yields a lower force. Labels '1 mm' and '3 mm' are used in Fig. 4 to denote the minimum and the maximum values of the piezoelectric-layer thickness investigated, respectively.

The results displayed in Fig. 4 also show that the simple analytical model defined by equations (10) and (11) predicts reasonably well the tip free displacement versus the tip blocked force relation in the actuators with constant-thickness piezoelectric layers especially at high values of the piezoelectric-layer thickness at which the neglect of the supporting layer is more justified.

3.2 Piezoelectric layer with linearly varying thickness

To explore further the trade-off between the tip free displacement and the tip blocked force, a number of plane-strain finite element simulations are carried out in which the thickness of the piezoelectric layers is assigned to vary linearly along the length of the bimorph actuator. In all these simulations, the average thickness of the piezoelectric layers is taken to be 2 mm. The following combinations of the piezoelectric-layer thickness at the fixed actuator end/piezoelectric-layer thickness at the free actuator end are analysed: 1 mm/3 mm, 1.5 mm/2.5 mm, 2 mm/2 mm, 2.5 mm/1.5 mm, 3 mm/1 mm and 3.5 mm/0.5 mm. The remaining geometrical and operational parameters are kept at their values as used in the previous section. The results of this simulation are shown in Fig. 5.

The results presented in Fig. 5 show that when the piezoelectric layers are relatively thin at the fixed end and relatively thick at the free end of the bimorph actuator (e.g. the 1 mm/3 mm case), the tip displacement is increased at the expense of the tip blocked force. As the actuator becomes thicker at the fixed end and thinner at the free end, the magnitude of the blocked force increases while that of the free displacement decreases. However, when the bimorph actuator becomes quite thick at the fixed end and quite thin at the free end, both the tip free displacement and the blocked force tend to increase with the fixed end over the free end thickness ratio of a

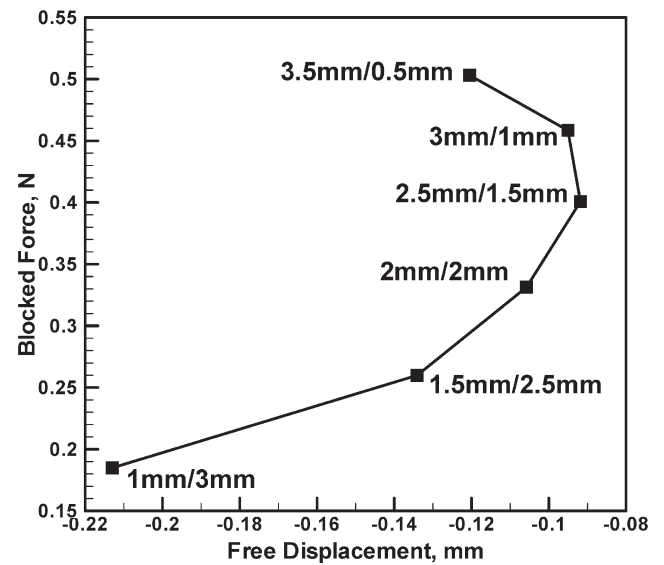


Fig. 5 A trade-off between the actuator-tip free displacement and the actuator-tip blocked force in bimorph actuators in which the thickness of their piezoelectric layers varies linearly with distance along the length of the actuator. The notation used, e.g. 1 mm/3 mm, denotes an actuator in which the thickness of a piezoelectric layer at the fixed end is 1 mm and its thickness at the free end is 3 mm

bimorph actuator. Unfortunately, when the thickness of the piezoelectric layer decreases, the electrical field through it increases and the polarization of the piezoelectric layers tends to approach its saturation value. Even before such saturation occurs, polarization versus field relation becomes nonlinear and the piezoelectric materials constitutive equations, discussed in section 2.1, become invalid. The linear piezoelectric constitutive model in PZT is generally accepted to be valid up to the field of about 1000 V/mm. This implies that the minimum allowed thickness of the PZT layer is $100 \text{ V}/1000 \text{ V/mm} = 0.1 \text{ mm}$.

3.3 Optimization of the morphology of a piezoelectric bimorph actuator

In this section, the results of the combined three-dimensional finite element and genetic algorithm optimization analyses of a piezoelectric bimorph actuator for use in minimally invasive surgical suture-needle holder applications is presented. In these analyses, each of the piezoelectric PZT layers is assumed to consist of five equal-length (10 mm), constant-thickness (between 1 mm and 3 mm) segments and four constant-length (1 mm) transition PZT segments with a linear variation of the thickness along the actuator length. In all these calculations, the PZT layers are assumed to be poled in the (through-the-thickness) 3-direction. A perfect bonding is assumed between the piezoelectric and the

supporting layers. The thickness of the supporting steel layer is assumed to be fixed at 0.75 mm, while the thicknesses of the five PZT segments are considered as design/optimization parameters. The objective function (which should be maximized through the use of the genetic algorithm presented in section 2.4) is defined as the bimorph actuator-tip deflection at a tip force of at least $0.25 \text{ N} = 0.5 \times (0.2 \text{ N} + 0.3 \text{ N})$. For a 0.5 mm diameter suture needle, Frecker *et al.* [7] estimated that the minimum grasping force should be 20–30 N per piezoelectric bimorph in order to ensure a safe and secure handling of the needle. That is the reason that a 25 N minimal grasping force has been identified as a functional constraint in the present optimization of the topology of the piezoelectric-bimorph-based suture-needle grasper. A maximum free-tip deflection has been selected as the objective function, since it is desirable that the suture-needle grasper has a maximum jaws opening since that ensures an easy grasping of the needle.

In order to obtain both the values of the tip displacement and the tip force, two identical springs (with a spring constant selected to match the bending stiffness of the bimorph actuator) are each attached to the points A and B in Fig. 3. A series of genetic algorithm optimizations is next carried out to

maximize the actuator tip deflection (at the points A and B). Since the tip force at the point A (or B) F_A is related to the corresponding tip displacement u_A , via the relation, $F_A = k_{\text{spring}} \times u_A$, where k_{spring} is the spring constant, any solution for which $u_A < 0.25 \text{ N}/2/k_{\text{spring}}$ is discarded as unacceptable since it does not meet the requirement for the minimal tip force of 0.25 N.

To ensure that a global maximum has been located, the genetic algorithm optimization procedure has been repeated ten times. It was found that, within the numerical accuracy of the FEMLAB and the MATLAB calculations, all ten simulations resulted in the same optimal morphology of the piezoelectric bimorph actuator.

The optimal morphology of the piezoelectric bimorph actuator is depicted in Fig. 6(a). The thicknesses of five constant-thickness PZT layers listed from the fixed end towards the free end of the actuator are: 2.5109, 1.8423, 1.1591, 1.0038, and 1.0246 mm. The associated tip displacement and the tip force are $u_A = 0.7658 \text{ mm}$ and $F_A = 0.25 \text{ N}$. Thus, the total grasper-jaws opening is $2 \times 0.7658 = 1.5316 \text{ mm}$ which is relatively small and may not be sufficient to ensure an easy grasp of the suture needle. Nevertheless, the tip displacement ($= 0.7658 \text{ mm}$) is more than three

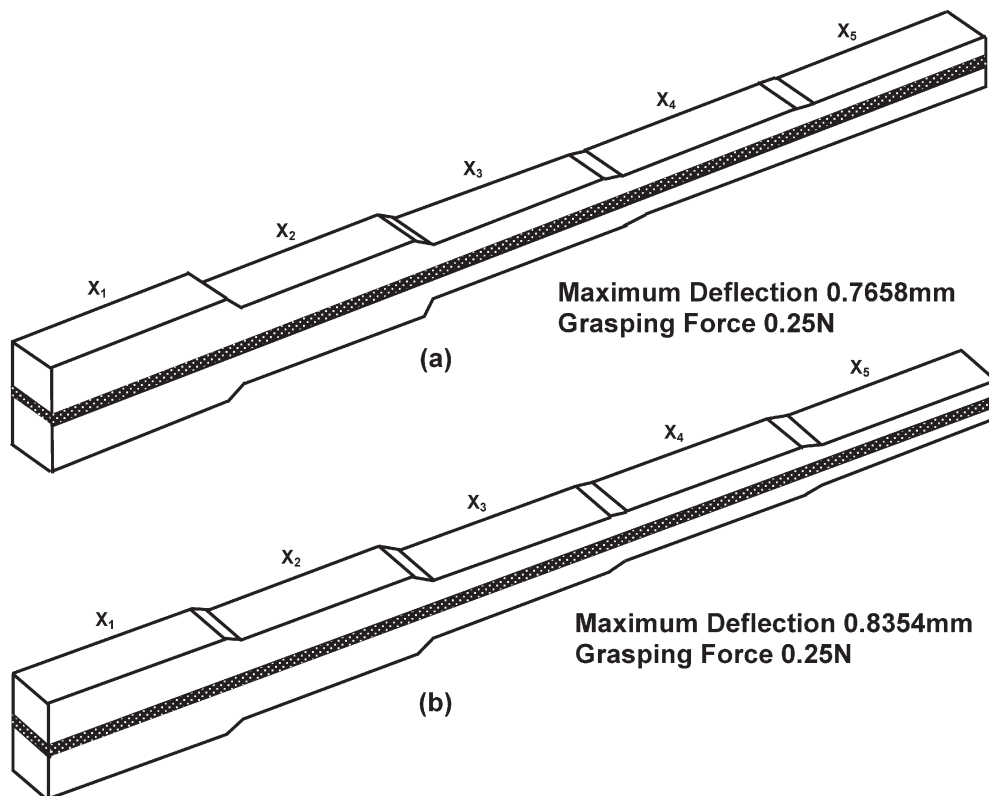


Fig. 6 Optimized morphologies of the piezoelectric bimorph actuator for minimally invasive surgery suture-needle grasper/holder applications: (a) a zero poling angle case and (b) the case when the poling angle is varied to obtain an optimal grasper performance. X_1 to X_5 are used to designate the thicknesses of the five constant-thickness segments of the piezoelectric layers

times larger than the largest on (~ 0.215 mm for 1 mm/3 mm) in Fig. 4 and also meets the minimal grasping force requirement (while the 1 mm/3 mm case in Fig. 4 does not meet the 0.25 N force requirement).

3.4 Effect of the poling direction on the bimorph-actuator performance

In all the calculations up to this point, the poling direction in the PZT layers was kept fixed and aligned with the through-the-thickness direction of the piezoelectric bimorph actuator. In this section, whether varying the poling direction relative to the through-the-thickness direction of the piezoelectric bimorph actuator can improve the performance of these devices. Only the variation of the poling direction in the 1–3 plane is considered in the present work. This variation is defined by the rotation angle β about the 2-direction (in the clockwise direction for the upper PZT layer and in the counterclockwise direction for the lower PZT layer of the top half of piezoelectric bimorph grasper, Fig. 2). Thus β represents an angle between the poling direction and the global 3-direction. Since the rotation is carried out about the 2-direction, the components of the materials stiffness matrix, c^E , the stress/field piezoelectric matrix, e , and the permittivity matrix, ε^S , associated with 2-direction are not altered as a result of this rotation. Consequently, the following reduced matrix equation, corresponding to equation (3) is introduced:

$$\begin{Bmatrix} T_{11} \\ T_{33} \\ T_{13} \\ D_1 \\ D_3 \end{Bmatrix} = \begin{bmatrix} C_{11} & C_{13} & C_{15} & 0 & -e_{31} \\ C_{13} & C_{33} & C_{35} & 0 & -e_{33} \\ C_{15} & C_{35} & C_{55} & -e_{15} & 0 \\ e_{11} & e_{13} & e_{15} & \varepsilon_{11} & 0 \\ e_{31} & e_{33} & 0 & 0 & \varepsilon_{33} \end{bmatrix} \begin{Bmatrix} S_{11} \\ S_{33} \\ 2S_{13} \\ E_1 \\ E_3 \end{Bmatrix} \quad (12)$$

or

$$\begin{bmatrix} T \\ D \end{bmatrix} = \begin{bmatrix} c^E & e^t \\ e & \varepsilon^S \end{bmatrix} \begin{bmatrix} S \\ E \end{bmatrix} \quad (13)$$

Following the standard procedure for transformation of the second- and fourth-order tensors, a rotation around 2-direction by an angle β , gives rise to the following transformations of the elastic and piezoelectric material property matrices:

$$c'^E = T_\varepsilon^t c T_\varepsilon \quad (14)$$

$$e' = \Lambda^t e T_\varepsilon \quad (15)$$

and

$$\varepsilon' = \Lambda^t \varepsilon \Lambda \quad (16)$$

where a prime is used to denote the appropriate quantities after rotation and the two rotation matrices are defined as:

$$\Lambda = \begin{bmatrix} \cos \beta & \sin \beta \\ -\sin \beta & \cos \beta \end{bmatrix} \quad (17)$$

and

$$T_\varepsilon = \begin{bmatrix} \cos^2 \beta & \sin^2 \beta & \cos \beta \sin \beta \\ \sin^2 \beta & \cos^2 \beta & -\cos \beta \sin \beta \\ -2 \cos \beta \sin \beta & 2 \cos \beta \sin \beta & \cos^2 \beta - \sin^2 \beta \end{bmatrix} \quad (18)$$

To explore the effect of orientation of the poling direction on the performance of piezoelectric bimorph actuators, the poling angle β is added as the sixth design/optimization parameter to the procedure described in the previous section and the genetic algorithm is reapplied. The results of this procedure are displayed in Fig. 6(b). The optimal thicknesses of the five constant-thickness PZT segments listed in the same order as in the previous section are: 2.5917, 1.9744, 1.4018, 1.1723, and 1.0012 mm. The optimal value of the poling angle is found to be approximately 2.3° . The corresponding actuator tip displacement and tip force are: $u_A = 0.8354$ mm and $F_A = 0.25$ N. This finding suggests that only an increase of about 10 per cent in the grasper-jaws opening is attainable by changing the poling angle of the PZT layers. However, the total grasper-jaws opening ($2 \times 0.8354 = 1.6708$ mm) is still relatively small. The observed effect of the poling angle on the maximum free-tip displacement is the result of the fact that when the poling angle does not coincide with the through-the-thickness direction of the piezoelectric bimorph, the dimensions of the bimorph undergo a change in both the length and the thickness direction. Dimensions of the bimorph also undergo a change in the width direction, but these changes are typically inconsequential for the functional operation of the grasper and are not considered any further. While the length change of the piezoelectric bimorph plays a dominant role on the free-tip displacement, dimensional changes in the through-the-thickness direction also have a measurable contribution to this displacement. When the poling direction is in the through-the-thickness direction, the piezoelectric bimorph undergoes only a change in the length direction. Hence, the optimal poling angle of 2.3° corresponds to the condition when the combined contributions of the length and thickness changes have a maximum contribution to the free-tip displacement of the bimorph actuator.

It should be noted that further increases in the PZT-based grasper-jaws opening can be achieved by

reducing the minimum thickness of the PZT layers and/or by increasing the magnitude of the applied voltage. According to equation (10), the tip free displacement is inversely proportional to the squared PZT-layer thickness and scales linearly with magnitude of the applied voltage. This implies that reducing the minimal PZT thickness by a factor of two and increasing the applied voltage by the same factor can increase the tip free displacement by a factor of eight. While this would significantly increase the magnitude of the grasper-jaws opening and enable an easy grasp of the suture needle, smaller PZT layer thicknesses may present manufacturability problems while higher values of the applied voltage are associated with safety concerns.

Another potential way for increasing the magnitude of the grasper-jaws opening is through an increase in the actuator width. According to equation (11), the actuator-tip blocked force increases linearly with its width. Thus, in wider graspers, the required level of the grasping force can be obtained in morphologies which are optimized with respect to maximizing the tip deflection. In fact, when the grasper width was doubled to 6 mm, the magnitude of the grasper-jaws opening is found to be 2.9406 mm, an increase by about 76 per cent.

4 CONCLUSIONS

Based on the results obtained in the present work, the following main conclusions can be drawn:

1. PZT-based piezoelectric bimorph actuators appear to be suitable for use in the minimally invasive surgery suture-needle grasper/holder applications.
2. To obtain a compromise between a high actuator-tip deflection encountered in actuators with thin piezoelectric layers and a high tip blocked force encountered in the actuators with thick piezoelectric layers, actuators with variable thicknesses of their piezoelectric layers should be used with the thickness variation along the actuator length optimized in order to maximize the grasper performance.
3. The use of the poling direction different from the one standard through-the-thickness direction to increase the grasper performance is found to have only a limited effect. An increase in the grasper width, of the other hand, can significantly increase the grasper-jaws opening to enable an easy grasp of the suture needle.

ACKNOWLEDGEMENTS

The material presented in this paper is based on work supported by the U.S. Army Grant Number

DAAD19-01-1-0661. The authors are indebted to Drs Walter Roy, Fred Stanton, Bryan Cheeseman, and William DeRosett of ARL for their support and a continuing interest in the present work. The authors also acknowledge valuable discussions with Mr James Gilbert of Clemson University.

REFERENCES

- 1 **Fatikow, S.** and **Rembold, U.** *Microsystem technology and microrobotics*, 1997 (Springer-Verlag, Berlin Heidelberg).
- 2 **Chonan, S., Jiang, Z. W., and Koseki, M.** Soft-handling gripper driven by piezoceramic bimorph strips. *Smart Mater. Struct.*, 1996, **5**, 407–414.
- 3 **Seki, H.** Piezoelectric bimorph microgripper capable of force sensing and compliance adjustment. Japan/USA Symposium on *Flexible Automation*. Vol. 1, 1992, (ASME), pp. 707–713.
- 4 **Bar-Cohen, Y., Leary, S., Shahinpoor, M., Harrison, J. O., and Smith, J.** Flexible low-mass devices and mechanisms actuated by electro-active polymers. *Proc. SPIE Smart Structures and Materials*, 1999, **3669**, 51–56.
- 5 **Lumia, R. and Shahinpoor, M.** Microgripper using electro-active polymers. *Proc. SPIE Smart Structures and Materials*, 1999, **3669**, 322–329.
- 6 **Cappelleri, D. J. and Frecker, M. I.** Optimal design of smart tools for minimally invasive surgery. Proceedings of *Optimization in Industry II*, Banff, Canada, June 1999.
- 7 **Frecker, M. I., Dziedzic, R. P., and Haluck, R. S.** Design of multifunctional compliant mechanisms for minimally invasive surgery. *Min. Invas. Ther. and Allied Technol.*
- 8 **Canfield, S., Edinger, B., Frecker, M., and Koopmann, G.** Design of piezoelectric inchworm actuator and compliant end effector for minimally invasive surgery. Proceedings SPIE 6th International Symposium on *Smart Materials and Structures*, Newport Beach, California, March 1999, Paper 3668-78.
- 9 **Sastry, S., Cohn, M., and Tendick, F.** Millirobotics for remote minimally invasive surgery. *Robot. Auton. Syst.*, 1997, **21**, 305–316.
- 10 **Balazs, M., Feussner, H., Hirzinger, G., Omote, K., and Ungeheuer, A.** A new tool for minor access surgery. *IEEE Engng Med. and Biol.*, 1998, May/June, 45–48.
- 11 **Smits, J. G., Dalke, S. I., and Cooney, T. K.** The constituent equations of piezoelectric bimorphs. *Sensors and Actuators*, 1991, **28**, 41–61.
- 12 **Soper, N. J., Brunt, L. M., and Kerbl, K.** Laparoscopic general surgery. *New England Journal of Medicine (NEJM)*, 1994, **330**(6), 409–419.
- 13 **Soper, N. J., Odem, R. R., Clayman, R. V., and McDougall, E. M.** (Eds), *Essentials of Laparoscopy*, 1994b (Quality Medical Publishing, Inc., St. Louis).
- 14 www.comsol.com, FEMLAB 3.0a, COMSOL Inc., Burlington, MA 01803, 2004.
- 15 **MATLAB**, *The Language of Technical Computing*, 6th Edition, 2003 (The MathWorks Inc., MA).
- 16 **Grujicic, M. and Chittajallu, K. M.** Design and optimization of polymer electrolyte membrane (PEM) fuel cells. *Appl. Surface Sci.*, 2004, **227**, 56–72.

- 17 **Goldberg, D. E.** Genetic algorithms in search, optimization and machine learning, 1989 (Addison-Wesley, Reading, MA).
- 18 **Grujicic, M., Cao, G., and Gersten, B.** Optimization of the chemical vapor deposition process for carbon nanotubes fabrication. *Appl. Surface Sci.*, 2002, **191**, 223–239.
- 19 **Benjeddou, A.** A unified beam finite element model for extension and shear piezoelectric actuation mechanisms, 1997 (Structural Mechanics and Coupled Systems Laboratory, CNAM, Paris, France).

APPENDIX 1

Notation

c	elastic stiffness matrix
d	strain/field piezoelectric matrix
D	electrical dipole vector
e	stress/field piezoelectric matrix
E	Young's modulus of the supporting layer
E	electric field vector
F	actuator-tip-blocked force
l	actuator length
s	elastic compliance matrix
S	strain vector
t	thickness of a single piezoelectric layer
T	stress vector
V	voltage
w	actuator width
β	polarization angle
δ	actuator-tip-free deflection
ε	permittivity matrix
ν	Poisson's ratio of the supporting layer

Subscripts

1, 2, 3	quantities associated with three global directions
ε	quantities specific to the piezoelectric material

Superscripts

E	constant-field condition
S	constant-strain condition
t	matrix transpose
'	material property in a $\beta \neq 0$ condition

APPENDIX 2

Elastic and piezoelectric properties of PZT

The following elastic and piezoelectric properties of PZT are used in the present work: these properties were taken from reference [19].

Constant-field elastic stiffness matrix

$$c^E = \begin{bmatrix} 126 & 79.5 & 84.1 & 0 & 0 & 0 \\ & 126 & 84.1 & 0 & 0 & 0 \\ & & 117 & 0 & 0 & 0 \\ & & & 23.3 & 0 & 0 \\ \text{sym} & & & & 23.0 & 0 \\ & & & & & 23.0 \end{bmatrix} \text{ GPa}$$

Stress/field piezoelectric constant matrix

$$e = \begin{bmatrix} 0 & 0 & 0 & 0 & 0 & 17 \\ 0 & 0 & 0 & 0 & 17 & 0 \\ -6.5 & -6.5 & 23.3 & 0 & 0 & 0 \end{bmatrix} \text{ C/m}^2$$

Constant-strain permittivity matrix

$$\varepsilon^S = \begin{bmatrix} 1.503 & 0 & 0 \\ 0 & 1.503 & 0 \\ 0 & 0 & 1.3 \end{bmatrix} \times 10^{-8} \text{ F/m}$$